

Sulfate removal from aqueous solutions using esterified wool fibers: isotherms, kinetic and thermodynamic studies

Fatine Akoh^{a,b}, Hayat Bouchoum^{a,b}, Mehdi El Bouchti^b, Omar Cherkaoui^b, Amane Jada^{c,d,*}, Mohamed Tahiri^a

^aGeosciences Laboratory, Faculty of Sciences Ain Chock, Hassan II University, B.P 5366 Maarif 20100, Casablanca, Morocco, emails: akoh.fatine@gmail.com (F. Akoh), bouchoum.hayat@gmail.com (H. Bouchoum), mohtahiri@yahoo.fr (M. Tahiri)

^bREMTEX Laboratory, Higher School of Textile and Clothing Industries, Casablanca, Morocco, emails: elbouchti@esith.ac.ma (M. El Bouchti), cherkaoui@esith.ac.ma (O. Cherkaoui)

^cUniversity Haute Alsace, CNRS, IS2M, UMR7361, F-68100 Mulhouse, France, email: amane.jada@uha.fr (A. Jada)

^dUniversity Strasbourg, Strasbourg, France

Received 14 August 2019; Accepted 17 January 2020

ABSTRACT

This work deals with the removal of sulfate ions from aqueous solutions onto modified wool fibers (WFs) used as adsorbent. The esterified wool fibers (EWFs) were prepared from the esterification of the pristine raw wool fibers (RWFs) by using methanol in the presence of HCl as a catalyst. Thereafter, we characterized the modified wool fibers by using various methods, such as titration for functionalization degree calculation, Fourier transform infrared spectroscopy and thermogravimetric analysis. Further, we studied parameters affecting sulfate removal from water onto both the EWFs and the RWFs, such as solution initial pH, initial concentrations, contact time, a mass of the adsorbent and the temperature. To assess the adsorption theoretical trends of sulfate ions from water onto the EWFs adsorbent, we compared the experimental adsorption results to Langmuir, Freundlich, and Dubinin–Radushkevich models. A good agreement was found between the experimental data and those predicted by the Langmuir model, which yielded a maximum monolayer adsorption capacity of 123.08 mg g⁻¹. Also, the adsorption kinetic results of the sulfate ions removal from water onto the EWFs adsorbent were found to follow a pseudo-second-order model. Finally, adsorption thermodynamic parameters including Gibbs free energy ΔG° , enthalpy ΔH° , and entropy ΔS° , have been estimated and showed that the sulfate ions adsorption onto the EWFs adsorbent is spontaneous, endothermic and favorable. The overall data indicate that the EWFs have economic and environmental advantages, since their uses are not limited only to adsorption but they can also be regenerated.

Keywords: Esterification; Methanol; Adsorption; Water; Regeneration

1. Introduction

Sulfate (SO₄²⁻) is a major ion present not only in natural waters but also in municipal and industrial wastewater [1]. The main natural sources of this ion, as well as, in aquatic surface and groundwater result from the chemical weathering process and the dissolution of naturally abundant

sedimentary sulfur minerals or evaporate rocks [2]. Other natural sources of SO₄²⁻ are the oxidation of sulfides and elemental sulfur, as well as the decomposition of animal and plant residues [3]. The presence of sulfate ions in the aquatic systems can also be anthropogenic. These ions are present in water via industrial effluents that use sulfuric acid or sulfate-rich compounds in their processes [4]. Sulfate ions have become one of the main industrial effluent components released in the

* Corresponding author.

aquatic environment, in addition to the waste resulting from industries such as mining, fuel oils, foundries, paper mills, textile mills, and tanneries [5]. It should be noted that when the amount of SO_4^{2-} exceeds 250 mg L^{-1} , it leads to plumbing corrosion, scaling of pipes and public water supplies, a bitter or astringent taste which may render the domestic water unpleasant to drink. When the ion concentration exceeds 600 mg L^{-1} , it causes a laxative effect, dehydration and gastrointestinal irritation on humans [6]. Also, high sulfate content in the water currents is dangerous because it promotes the formation of hydrogen sulfide and other toxic substances which can deteriorate aquatic life and harm the environment [7,8]. Thus, water desulphurization has attracted a lot of attention, and various water treatment approaches such as adsorption, precipitation, bioelectrochemical processing, aerobic and anaerobic processes, reverse osmosis, barium or calcium precipitation, membrane technology processes, were investigated [9–11]. Note that among these different methods, adsorption is considered to be an effective treatment for removing sulfate due to its efficiency over a wide range of substances, easy handling and relatively low cost of operation [6]. Recently, natural adsorbents, such as wetland plants, Pampas Grass (*Cortaderia selloana*) and Lucky Bamboo, were used to remove SO_4^{2-} from water. They were used in hydroponic cultivation systems for the treatment of simulated high-sulfate wastewaters [12]. Natural wool keratin fibers are among the most popular and cheap biopolymers and are usually used for their various specific properties such as elasticity handle, warmth retention, fullness, flexibility, ease of operation, simplicity, low cost, insensitivity to the characteristics of toxic pollutants, and importance of the fibers surface [13]. The wool fiber consists of polar and ionizable groups on the side chain of amino acid residues able to bind other charged organic and inorganic molecules [13]. In this study, wool fibers have been used as an adsorbent to remove (SO_4^{2-}) from aqueous solutions.

The modification of the wool chemical structure would be necessary by introducing new functional groups to increase the number of binding sites [13]. Scientific sources present several functionalization of wool fibers to improve adsorption properties such as the copolymerization of acrylic acid [14] methacrylic acid and acrylamide [15], treatment by citric acid [16] and modification with TiO_2 nanoparticles [17]. In this study, the modification was conducted by esterification of wool fibers with methanol in the presence of HCl as an acid catalyst [18]. In this experiment, the changes in the wool properties are mainly due to the appearance of new functional groups in the presence of HCl. This later will significantly enhance the esterification rate and leads to the decrease of the carboxyl groups that cause the repulsion between the surface of the wool and the sulfate ions. Consequently, the esterification of the wool will produce materials having a strong affinity to sulfate ions in aqueous solutions. The esterification is used in the textile industry to finish the wool fibers and to improve dyeing properties towards acid dyes [18], but in our case, esterified wool fibers (EWFs) were used as a good and low-cost adsorbent.

2. Materials and methods

2.1. Raw wool fibers

The raw wool fibers (RWFs) used in the present work, were purchased from Timahdite region (Morocco). Before

their uses, they were cleaned and then cut into small pieces. The impurities contained in fibers were removed by a extracting the fibers in a Soxhlet apparatus with distilled water for a period of 6 h.

2.2. Esterification

The RWFs were esterified with methanol containing hydrogen chloride, at wool/liquor weight ratio of 1/50. Reactions were carried out in a water bath with a reflux heating at 65°C , for various times from 1 to 6 h, and then the EWFs were rinsed with distilled water, dried, characterized and finally used for our adsorption experiments.

2.3. Functionalization degree calculation

0.1 g of EWFs or RWFs were added to 50 mL of NaOH (0.05 M). The mixture was stirred for 30 min, then filtered and the non-reacted NaOH was titrated back with HCl having a known concentration (0.05 M). The consumed NaOH amount by the EWFs or the RWFs should be equivalent to the amount of the fiber's carboxyl groups. Thus, the difference between the initial NaOH, and the HCl titrated NaOH, represents the quantities correspond to the fiber's carboxylic group amount. The fiber's functionalization degree was then calculated according to Eq. (1) [19]:

$$\frac{C_b(M)V_b(\text{ml}) - C_a(M)V_a(\text{ml})(\text{mmols})}{\text{Sample weight (g)}} \quad (1)$$

where C_b , V_b , C_a and V_a are, respectively, the basic solution (NaOH) initial concentration, the basic solution (NaOH) initial volume, the acidic solution (HCl, titrant) initial concentration and the volume of the acid solution consumed by the basic solution at the equivalent point. In Eq. (1), the sample weight represents the amount of EWFs, or RWFs used in the titration. Eq. (2) as shown below was used to calculate the reduced percentage of the carboxylic functions:

$$\frac{\text{mmols(RWFs)} - \text{mmols(EWFs)}}{\text{mmols(RWFs)}} \times 100 \quad (2)$$

2.4. Fourier transform infrared spectroscopy analysis

The recording of the Fourier transform infrared spectroscopy (FTIR) spectra of the studied samples was conducted using the Nicolet iS10FTIR-ATR spectrophotometer, combined with the Golden Gate single attenuated total reflection (ATR) accessory. The range of experiments took place between $4,000\text{--}400 \text{ cm}^{-1}$ with a 4 cm^{-1} resolution along with an accumulation of 32 scans.

2.5. Thermogravimetric analysis

Thermogravimetry/Derivative Thermogravimetry (TG/DTG) experiments were performed with a thermogravimetric analyzer (Cahn VersaTherm) to evaluate the thermal stability of the studied samples. The tests were achieved at a temperature ranging from 25°C to 700°C , with a heating rate of $20^\circ\text{C min}^{-1}$, and under an air atmosphere at a flow rate of 25 mL min^{-1} .

2.6. Synthetic water and adsorption

The pH measurements were made with a pH meter (Orion 4 Star). The UV spectroscopy (Evolution 300) was used to analyze the ions concentration in the synthetic solution, which was prepared with sodium sulfate (Na₂SO₄) obtained from Sigma-Aldrich (80 Rue de Luzais, 38070 Saint-Quentin-Fallavier, France).

A stock solution of SO₄²⁻ at 2,000 mg L⁻¹ concentration was prepared by dissolving 2.96 g of Na₂SO₄ in 1,000 mL of bi-distilled water.

After the esterification process, we investigated the adsorption properties of both RWFs and EWFs for comparison. Thus, the adsorption experiments were carried out by mixing 1 g of RWFs or EWFs with 200 mL of the SO₄²⁻ synthetic solution and the resulted mixtures were shaken at 500 rpm. In these adsorption experiments, many parameters were varied such as the initial pH (pH = 1–10); the initial sulfate concentration, C₀ (C₀ = 500–2,000 mg L⁻¹); the contact time adsorbate-adsorbent, t (1–60 min); the adsorbent masse, m (m = 1–12 g); and the adsorption temperature, T (T = 4°C–40°C).

The treated aqueous solution containing sulfate and fiber was separated by filtration using Whatman’s filter paper. Thereafter, the remaining sulfate ions present in the supernatant were precipitated with an aqueous solution containing a mixture of hydrochloric acid and barium hydroxide. The resulted precipitate in the form of barium sulfate (BaSO₄) was then stabilized with a surfactant solution of Tween 20. Thereafter, the absorbance values of homogeneous suspensions containing BaSO₄ were measured using UV/visible spectrometer at a wavelength, λ = 650 nm, using the calibration curve performed with a range of known SO₄²⁻ concentrations [20]. The pH values of various aqueous solutions were adjusted by using calibrated NaOH or HCl aqueous solutions.

The sulfate removal percentage (%) and the adsorption capacity (mg g⁻¹) were calculated, respectively, by using Eqs. (3) and (4):

$$\text{Removal (\%)} = \left[\frac{(C_0 - C_e)}{C_0} \right] \times 100 \tag{3}$$

$$Q_e = V \times \left[\frac{(C_0 - C_e)}{m} \right] \tag{4}$$

where C₀ (mg L⁻¹) and C_e (mg L⁻¹) are the initial and the equilibrium sulfate concentrations, respectively, Q_e (mg g⁻¹) is the equilibrium adsorbed amount, V (L) is the volume of synthetic solution and m (g) is the adsorbent mass.

2.7. Regeneration study

After the adsorption experiments, the reusability of the EWFs adsorbent was investigated. Thus, various aqueous solutions of pH = 4, pH = 7 and pH = 9, were used to desorb SO₄²⁻ from EWFs, and the number of adsorption-desorption cycles was assessed. In these experiments, a given adsorbent amount (1 g) was first mixed with 200 mL of sulfate solution at optimum conditions. Thereafter, the SO₄²⁻ ions were desorbed

using the above-mentioned pH solutions for 1h at the room temperature. After the desorption process, the adsorbent was recovered by filtration, washed by distilled water, and dried to be reused for the next adsorption-desorption cycles.

In order to determine the desorption rate, the following calculation was conducted [21].

$$\text{Desorption (\%)} = \left(\frac{Q_{\text{desorbed}}}{Q_{\text{adsorbed}}} \right) \times 100 \tag{5}$$

3. Results and discussions

3.1. Characterization of EWFs

3.1.1. Functionalization degree calculation

A simple titration method has been applied for the quantitative characterization of carboxylic functions on EWFs and RWFs [19]. This method is accurate, non-destructive, and fast. The calculated results are summarized in Table 1. The HCl titration of the non-consumed NaOH by the wool fiber shows a reduction of the carboxylic group’s amount as a function of the esterification time from 1.7 to 0.6 mmol g⁻¹, indicating a reduction percentage of 63% (Fig. 1). Such reduction of the carboxyl groups upon esterification of the fiber is due to a decrease in the consumption of NaOH by the wool fibers, which explains the achievement of the esterification reaction [19].

3.1.2. FTIR analysis

We recorded the RWF and EWFs FTIR spectra in order to obtain information about the nature of the functional groups added on the modified wool fibers surface resulting from the esterification process. As can be seen in Fig. 2, there is an additional band from newly formed esters functional group “C=O”, successfully resulted from the wool fibers surface modification by methanol, leading to a peak occurring at 1,731 cm⁻¹. Moreover, the “C-H” peak intensity occurring at 2,929 cm⁻¹ has tremendously increased due to the aliphatic

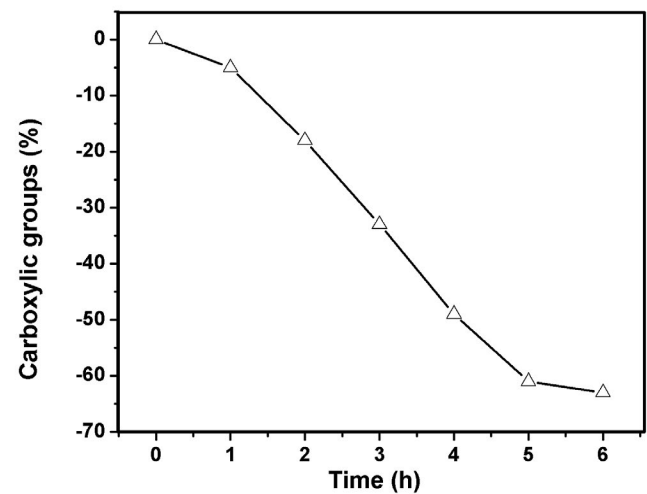


Fig. 1. Reduction of carboxylic functions vs. the esterification time.

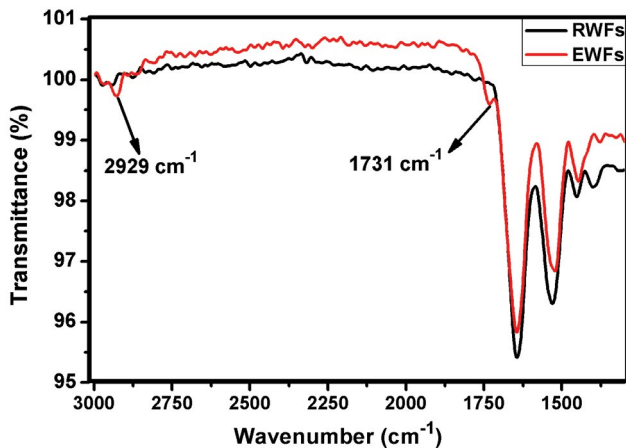


Fig. 2. FTIR spectra of RWFs and EWFs at optimum conditions (Wool/liquor weight ratio: 1/50; time = 6 h; $T = 65^{\circ}\text{C}$).

acid chain associated with the dodecanoyl fraction incorporated in fiber molecules [22].

3.1.3. Thermogravimetric analysis

The thermogravimetric analysis (TGA) of wool fibers before and after esterification allows us to monitor the degradation of the samples at high temperatures and to estimate their thermal stability in different types of water such as industrial wastewater rich in sulfate ions.

Figs. 3a and b show the TGA curves of the RWFs and EWFs heated up to 700°C . $T_{\text{max}1}$ (Temperature while the maximum first weight loss occurred), $T_{\text{max}2}$ (Temperature while the second maximum weight loss occurred), the residue at $T = 700^{\circ}\text{C}$ and the residual weight are gathered in Table 2. As can be observed in Fig. 3, the weight loss of the wool fibers primarily appears at three steps, from 50°C to 115°C , 200°C to 315°C , and 315°C to 700°C . However, important weight loss occurs between 315°C and 700°C . The first stage of the weight loss occurring from 50°C to 115°C , is attributed to decreases of, respectively, 5% and 15%, due to the loss of water physically bound to the wool, recalling that the moisture content of wool at 65% relative humidity is 11% [23]. The weight loss in the case of EWFs is 3 times that of RWFs since the ester groups (OCOCH_3) in the EWFs are retaining more water than do the carboxylate groups ($\text{O}=\text{C}-\text{O}-$) in the RWFs. Such water retention on the EWFs results from the hydrogen bonding occurring between water molecules and the ester groups ($\text{O}=\text{C}-\text{O}-\text{CH}_3$). The esterification reaction of the wool fibers likely makes them more hydrophilic [24]. The second stage of weight loss, between 220°C to 400°C , is characterized by a 24% reduction at 288.6°C and 311°C for RWFs and EWFs respectively. The weight loss is associated with the hydrogen bonds rupture of the peptide helical structure, cross-linking through condensation reaction and the ordered regions experienced a solid to melted phase change [23,25]. The cleavage of the disulfide bonds occurs along with emission of few volatile gasses including hydrogen sulfide gas and sulfur dioxide [23,25]. This is the stage where the fastest rate of weight loss is detected. Along this process, the structure of wool is

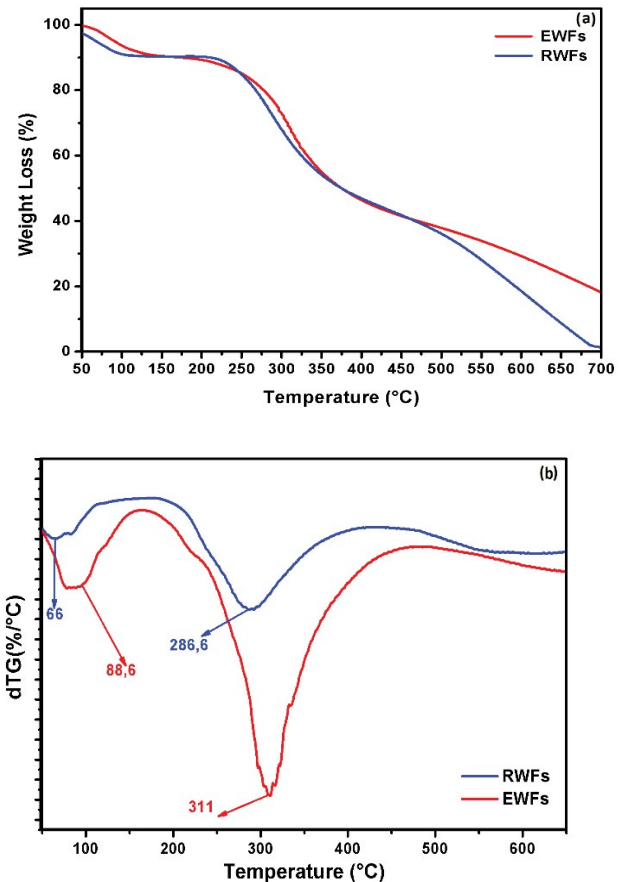


Fig. 3. (a) TG and (b) DTG curves of RWFs and EWFs at optimum conditions (Wool/liquor weight ratio: 1/50; time = 6 h; $T = 65^{\circ}\text{C}$).

Table 1
Carboxyl groups amount of RWFs and EWFs (Wool/liquor weight ratio: 1/50; time = 6 h; $T = 65^{\circ}\text{C}$)

Esterification time (h)	Amount of carboxylic functions (mmol g^{-1})	
	RWFs	EWFs
0	1.7	1.7
1	–	1.6
2	–	1.5
3	–	1.5
4	–	0.9
5	–	0.65
6	–	0.6

broken down through breaking down various chain linkages, peptide bridges and other lateral chains that ultimately lead to a skeletal breakdown of the fiber. During the third stage, weight loss takes place quite slowly, since most of the organic part is decomposed, moreover, the last loss is corresponding to the pyrolytic decomposition region (above 400°C), there is a severe contraction due to cyclization for RWFs and EWFs [25]. However, the biggest degradation is for RWFs

Table 2
Thermogravimetric data of RWFs and EWFs (Wool/liquor weight ratio: 1/50; time = 6 h; $T = 65^{\circ}\text{C}$) in air atmosphere

Samples	T_{max1} ($^{\circ}\text{C}$)	Residue at T_{max1} (%)	T_{max2} ($^{\circ}\text{C}$)	Residue at T_{max2} (%)	Residue at 700°C (%)
RWFs	66	95	286.6	73.06	1.38
EWFs	88.6	74.93	311	73.45	18.63

with a residue of 1.38% as a result of the decarboxylation of carboxyl groups and this explains the strong thermal stability of EWFs (18.63% residue).

3.2. Adsorption parameters

3.2.1. Effect of pH

The solution's initial pH is an important parameter that must be considered during an adsorption study. The effect of this parameter on the adsorption capacity was analyzed using pH ranging from 1.0 to 10.0, an initial concentration of $1,000 \text{ mg L}^{-1}$ of SO_4^{2-} solution and initial adsorbent amount of 5 g L^{-1} of RWFs or EWFs at room temperature. Note that the solution's initial pH affects not only the surface charge of the adsorbent but also provides information on sulfates chemical speciation in aqueous solutions. According to the literature of sulfur compounds [26], when $\text{pH} < 2$, the most dominant element is HSO_4^- and when $\text{pH} > 2$, sulfur exists as SO_4^{2-} . Fig. 4 reveals that at pH 2.0 the SO_4^{2-} ions reach their highest adsorption capacities of 26.78 mg g^{-1} and 45.78 mg g^{-1} , for respectively, RWFs and EWFs. The low adsorption capacity of the RWFs is due to electrical repulsion between the carboxyl groups and the sulfate molecules [27,28], whereas, the EWFs adsorbent demonstrates high adsorption capacity since the ester groups do not repel the SO_4^{2-} ions, due to their low chemical reactivity, as compared to carboxyl groups [18] (Fig. 5). Increasing the initial pH values from 3.0 to 4.0 leads to a decrease in the adsorption capacity of SO_4^{2-} from 5.88 to 0.024 mg g^{-1} for RWFs and from 15.48 to 3.22 mg g^{-1} for EWFs. Such adsorption behaviors can be explained as follows:

- When $2 \leq \text{pH} < 3$, the adsorbent surface containing amino groups becomes protonated to a high level and forms more positively surface charges that exert a strong electrostatic attraction on SO_4^{2-} (which is the dominant form in the solution).
- When $\text{pH} > 3$, a decrease in adsorption capacity is created by the deprotonation of functional groups on the adsorbent surface negatively charged, causing hence an electrostatic repulsion and a competition between the OH^- and SO_4^{2-} ions leading to less adsorption of the sulfate groups [27,28]. Thus, the next adsorption experiments will be operated at $\text{pH} = 2$.

3.2.2. Effect of initial concentrations

Fig. 6 shows the effect of SO_4^{2-} initial concentrations on the adsorption capacity using the optimal pH for 1h. Based on these experiments, the higher the SO_4^{2-} concentration, the higher are the adsorption capacities of RWFs and EWFs. In other words, more the solution is concentrated in SO_4^{2-} , more is the sulfate ions adsorption capability and better is the

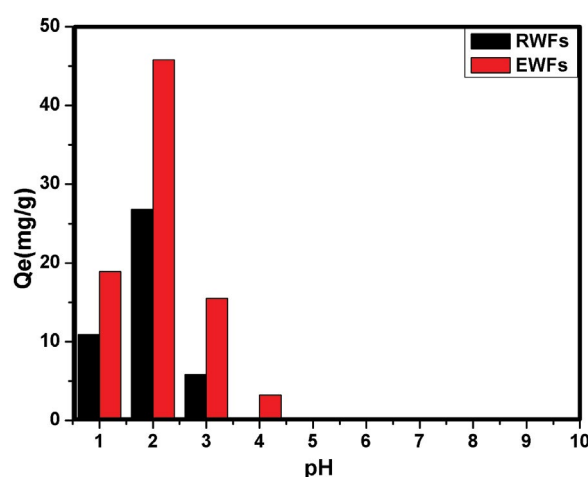


Fig. 4. Effect of pH ($[\text{SO}_4^{2-}] = 1,000 \text{ mg L}^{-1}$; $T = 25^{\circ}\text{C}$; $t = 60 \text{ min}$, 5 g L^{-1}).

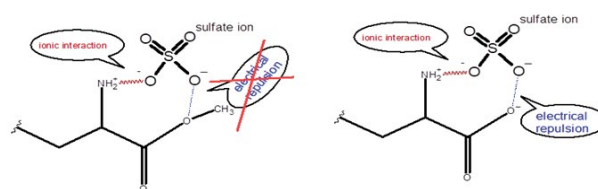


Fig. 5. Adsorption mechanism before and after esterification.

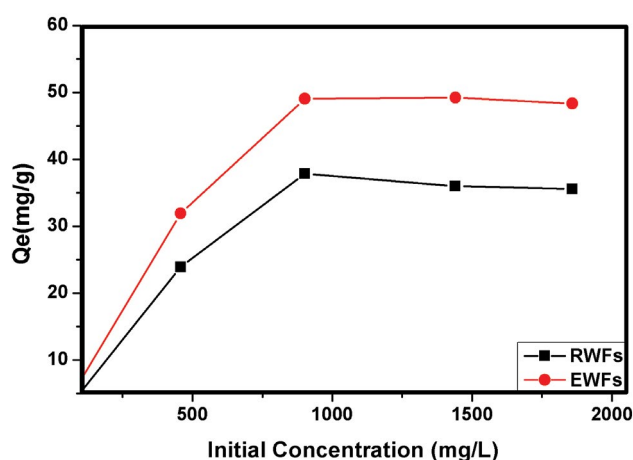


Fig. 6. Effect of initial concentrations ($\text{pH} = 2$; $T = 25^{\circ}\text{C}$; $t = 60 \text{ min}$, 5 g L^{-1}).

interaction adsorbate-adsorbent [29,30]. Further, in Fig. 6, the SO_4^{2-} adsorption levels at adsorbate concentration of $1,000 \text{ mg L}^{-1}$ and becomes constant afterward. Such adsorption behavior can be explained by the saturation of the adsorbent active surface sites above this SO_4^{2-} initial concentration. As can be observed in Fig. 6, the reached SO_4^{2-} ions adsorption capacities at equilibrium are 22 mg g^{-1} for RWFs and 49 mg g^{-1} for EWFs. From these adsorption data, it is obvious that the EWFs has better adsorption capacity as compared to RWFs. According to the adsorption data presented in Fig. 6, the following experiments will be performed at $1,000 \text{ mg L}^{-1}$ of SO_4^{2-} .

3.2.3. Effect of the contact time adsorbate-adsorbent

Fig. 7 illustrates the contact time effect on the SO_4^{2-} ions adsorption from water onto the RWFs and EWFs fiber surfaces. The adsorption data show that the retention time of the sulfate ions is relatively fast. Hence, after 1 min of the contact time, the adsorption capacities reached are 13.43 and 20.5 mg g^{-1} , respectively, RWFs and EWFs. When the contact time adsorbate-adsorbent increases, the adsorbed

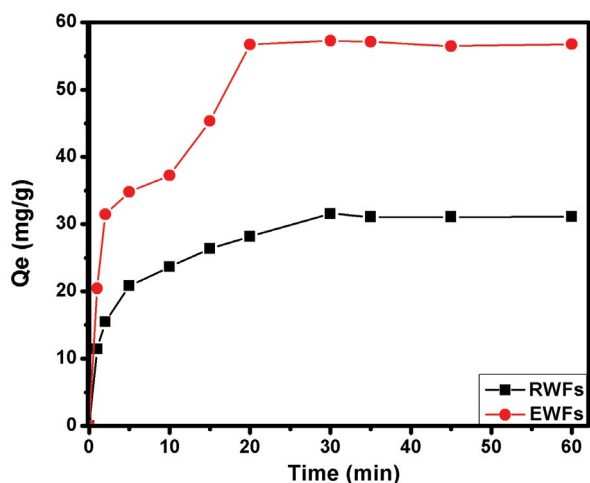


Fig. 7. Effect of contact time ($[\text{SO}_4^{2-}] = 1,000 \text{ mg L}^{-1}$; $T = 25^\circ\text{C}$; $\text{pH} = 2, 5 \text{ g L}^{-1}$).

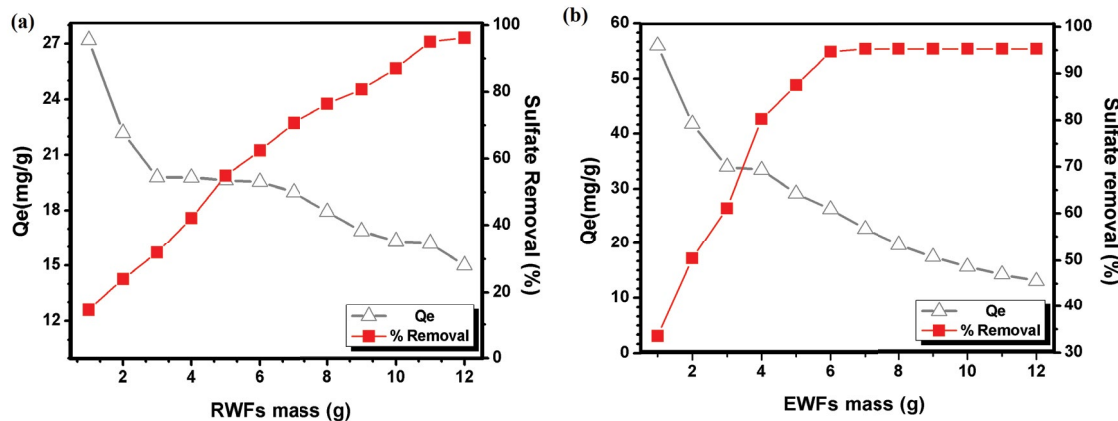


Fig. 8. Effect of RWFs (a) and EWFs (b) mass ($[\text{SO}_4^{2-}] = 1,000 \text{ mg L}^{-1}$; $\text{pH} = 2$; $T = 25^\circ\text{C}$; $t = 20 \text{ min}$ (EWFs); $t = 30 \text{ min}$ (RWFs)).

amount increases for both samples and reaches maximums of 31.55 mg g^{-1} after 30 min of elapsed contact time for RWFs, and 56.75 mg g^{-1} after 20 min of contact time for EWFs. In conclusion, longer is the contact time, less is the available surface sites, leading hence to the adsorption capacity to continue being constant for the remaining time [31,32]. This experiment also proves that the adsorption process of EWFs is faster than the RWFs one. Based on the previous results, the following experiments will be conducted at 30 and 20 min for RWFs and EWFs respectively.

3.2.4. Effect of the adsorbent mass

In order to estimate the optimum amount of the EWFs and RWFs to be added to the aqueous solution for removing all the sulfates, this experiment was conducted using 200 mL of synthetic water at concentration ($1,000 \text{ mg L}^{-1}$). Figs. 8a and b show that the increase in adsorbent mass of both RWFs and EWFs leads to a decrease of their adsorption capacities from 27.18 to 15.06 mg g^{-1} for RWFs and from 55.98 to 13.2 mg g^{-1} for EWFs. The decrease in Q_e values is mainly due to the increase of the adsorbent mass and the decrease of the ratio between the sulfate molecules and the adsorption sites number. On one hand, this Q_e decrease is typical and indicates, according to the literature study [29], that only active amino groups are involved in the adsorption process, while the inside particles remain inaccessible for interactions with sulfates. On the other hand, the elimination percentages values have remarkably increased from 14.47% to 96.14% for RWFs Fig. 7a and 33.67% to 95.3% for EWFs Fig. 7b, it means that the adsorbent mass increase can improve significantly the sulfate adsorption and let us get an optimal adsorbent mass of 11 and 6 g for RWFs and EWFs respectively to be used for sulfate removal and this ultimately indicates that EWFs generate more active sites than RWFs.

3.3. Adsorption isotherms of EWFs

The equilibrium adsorption modeling consists of relating the amount of the adsorbate in the liquid phase C_e (mg L^{-1}) and that adsorbed on the adsorbent surface Q_e (mg g^{-1}) is shown in Eq. (6). In the present work, the adsorption data at the equilibrium was analyzed by applying the Langmuir,

Freundlich and Dubinin–Radushkevich models, which are commonly used by researchers to investigate the adsorption isotherms of the adsorbent/adsorbate systems [31,33].

$$Q_e = V \times \left[\frac{(C_0 - C_e)}{m} \right] \tag{6}$$

3.3.1. Langmuir isotherm model

The theory of the Langmuir isotherm describes quantitatively the formation of a monolayer of the adsorbate on the adsorbent outer surface, which takes place on homogeneous specific adsorbent sites. Here, the sulfate adsorption isotherms from water onto EWFs were fitted by the Langmuir model as represented by Eq. (7):

$$\frac{C_e}{Q_e} = \frac{C_e}{Q_{\max}} + \frac{1}{K_L Q_{\max}} \tag{7}$$

where C_e (mg L⁻¹) is the adsorbate equilibrium concentration, Q_e (mg g⁻¹) is the adsorbate adsorbed amount at the equilibrium, K_L (L mg⁻¹) is the equilibrium constant relative to the Langmuir model, and Q_{\max} (mg g⁻¹) is the maximum adsorbed amount. The values of Q_{\max} and K_L are determined (Fig. 9), respectively, from the intersection with the y -axis and the slope of the line $C_e/Q_e = f(C_e)$ [12].

The data show that the correlation coefficient ($R^2 = 0.99$) of the Langmuir model is very close to unity (Table 3). Also, the use of the linear regression of Eq. (8) has allowed the determination of the maximum adsorption capacity Q_{\max} and the Langmuir equilibrium adsorption constant, K_L

which are, respectively, of the order of 123.08 mg g⁻¹ and 4.3×10^{-4} L mg⁻¹.

Note that an essential feature of the Langmuir isotherm may be expressed in terms of a dimensionless constant called the separation factor, R_L , defined by Eq. (8) below:

$$R_L = \frac{1}{1 + K_L C_0} \tag{8}$$

where C_0 (mg L⁻¹) is the adsorbate initial concentration and K_L is the Langmuir constant (L mg⁻¹). Hence, a separation factor $R_L > 1$ indicates that the adsorption is unfavorable, whereas if $R_L = 1$ the adsorption is linear; if $0 < R_L < 1$, the adsorption is favorable, and finally, if $R_L = 0$, the adsorption is irreversible. In the present work, the R_L value lies is between 0 and 1, which indicates a favorable adsorption reaction.

3.3.2. Freundlich isotherm model

The Freundlich isotherm model makes the assumption that the adsorption is multilayer and that the adsorbent surface is heterogeneous Eq. (9). The Freundlich model can be expressed following Eq. (9) [31,33]:

$$\ln Q_e = \ln k_f + \frac{\ln C_e}{n} \tag{9}$$

Thus, the plot of $\ln(Q_e)$ vs. $\ln(C_e)$ for SO_4^{2-} adsorption from water onto EWFs was found to be linear with a slope equal to $1/n$ and an intercept equal to $\ln(K_f)$ (Fig. 10). It should be recalled that the constant n is related to the

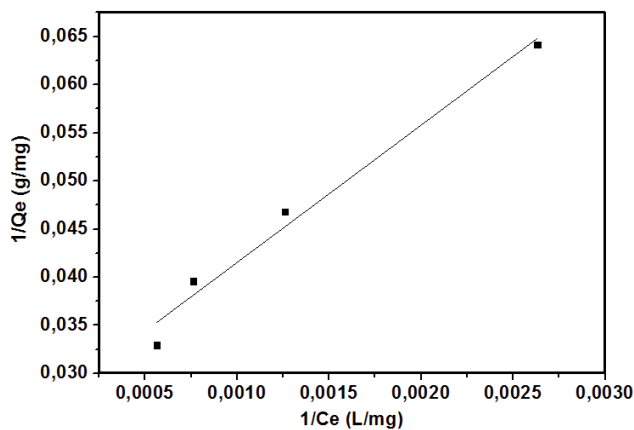


Fig. 9. Langmuir adsorption isotherm for SO_4^{2-} removal on EWFs.

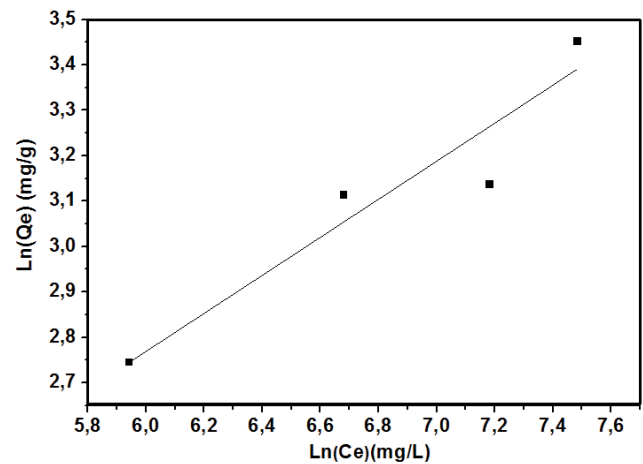


Fig. 10. Freundlich adsorption isotherm for SO_4^{2-} removal on EWFs.

Table 3 Isotherm models

Langmuir			Freundlich			Dubinin–Radushkevich		
Q_m (mg g ⁻¹)	K_L (L mg ⁻¹)	R^2	n	K_f (mg g ⁻¹)	R^2	Q_m (mg g ⁻¹)	E (kJ mol ⁻¹)	R^2
123.08	4.3×10^{-4}	0.99	1.39	0.2	0.88	2.73	5.9	0.81

adsorption intensity occurring between the adsorbent and the adsorbate, and it provides the adsorption behavior. Thus, if $n = 1$, the adsorption is linear; if $n < 1$, the adsorption is a chemical process; if $n > 1$, then adsorption is a physical process [31,33]. The Freundlich constant K_F (mg g^{-1}) is related to the adsorption capacity. Hence, as the K_F value increases, the adsorption capacity increases. The numerical values of K_F and n , assessed respectively, from the intercept point and the slope of the isotherm linear curve in Fig. 10, are presented in Table 3. However, as shown in Table 3, the correlation coefficient value R^2 is equal to 0.88, indicating that Freundlich model cannot describe the adsorption of SO_4^{2-} on the EWFs.

3.3.3. Dubinin–Radushkevich (D–R) isotherm model

The D–R isothermal model is applied for adsorbents having homogeneous and heterogeneous surfaces. According to this model, the calculated value of the adsorption energy gives information on the physical or the chemical nature of the adsorption process (Eq. (10)). Thus, the linearized form of the D–R isotherm model is given by Eq. (10) [32]:

$$\ln Q_e = \ln Q_m - \beta \varepsilon^2 \quad (10)$$

where Q_e (mg g^{-1}) is the adsorbed amount at the equilibrium, Q_m (mg g^{-1}) is the maximum adsorption capacity, β is a constant related to the mean free sorption energy E (kJ mol^{-1}) and ε is the Polanyi potential. ε and E are expressed by Eqs. (11) and (12), respectively;

$$E = \frac{1}{\sqrt{2\beta}} \quad (11)$$

$$\varepsilon = RT \ln \left(1 + \frac{1}{C_e} \right) \quad (12)$$

where R ($8.314 \text{ J mol}^{-1} \text{ K}^{-1}$) is the gas constant, T (K) is the absolute solution temperature.

Q_m and β ($\text{mol}^2 \text{ Jol}^{-2}$) can be calculated, respectively, from the intercept and the slope of the plot of $\ln Q_e$ vs. ε^2 (Fig. 11). This adsorption potential varies according to the nature of the adsorbent and the adsorbate, but it is independent of the temperature. The magnitude of E is used to define the type of adsorption mechanism. Hence, if $8 < E < 16$ (kJ mol^{-1}), the adsorption process is chemical in nature and if $E < 8$ (kJ mol^{-1}) the adsorption process is of a physical in nature [32].

We have analysed the adsorption data according to the Dubinin–Radushkevich isotherm model. Accordingly, as can be seen in Table 3, the correlation coefficient ($R^2 = 0.81$) is low, indicating that the D–R model may not be applied to SO_4^{2-} adsorption onto EWFs. Previous studies have reported that the adsorption of SO_4^{2-} is best described by Langmuir isotherm model [34,35], in a good agreement with our findings.

3.4. Adsorption kinetics of EWFs

Upon the mixture of various aqueous solution constituents, the adsorption of the sulfate ions from water onto the EWFs takes place and levels when the equilibrium is reached.

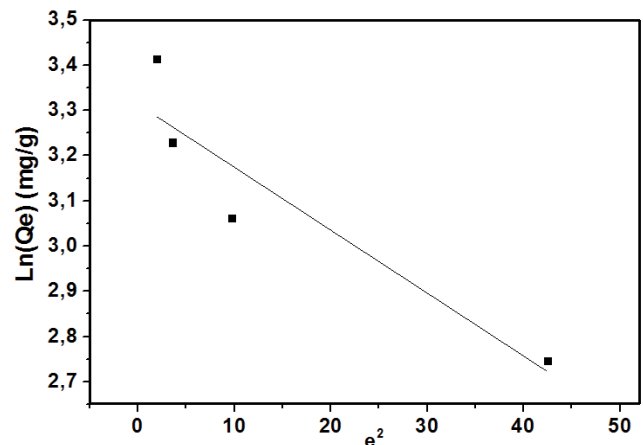


Fig. 11. Dubinin–Radushkevich adsorption isotherm for SO_4^{2-} removal on EWFs.

In this process, the adsorption reaction rate depends not only on the diffusion rate of the adsorbate from the bulk solution to the fiber surface, but also on the adsorbent-adsorbate interaction.

The adsorption kinetic study of the sulfate ions from water onto the EWFs allows us to examine the influence of contact time on the adsorbate retention. In the present work, two adsorption kinetic models [29,32], namely the pseudo-first-order Eq. (13), and the pseudo-second-order Eq. (14), have been used to describe the sulfate adsorption on EWFs:

$$\log(Q_e - Q_t) = \log Q_e - \frac{k_1 t}{2.303} \quad (13)$$

$$\frac{t}{Q_e} = \left(\frac{1}{Q_e} \right) t + \frac{1}{k_2 Q_e^2} \quad (14)$$

where Q_e and Q_t , expressed in mg g^{-1} , are the sulfate adsorbed amount, respectively, at equilibrium and at time t ; k_1 (min^{-1}) and k_2 ($\text{g mg}^{-1} \text{ min}^{-1}$) are the rate constants of, respectively, the first-order and the second-order adsorption reaction. The constant (k_1) and (k_2) for sulfate adsorption were calculated from the slope of the linear plots of, respectively, $\log(Q_e - Q_t)$ and (t/Q_e) vs. time as shown in Figs. 12a and b. The values of k_1 and k_2 obtained from first and second-order pseudo-kinetic models are gathered in Table 4. Also, taking into account the fact that the first-order kinetic model is not perfectly linear ($R^2 = 0.93$, Fig. 12a), whereas the second-order model is more applicable since the correlation coefficient ($R^2 > 0.99$, Fig. 12b) is very close to 1. Consequently, the pseudo-second-order adsorption model seems to be more suitable for describing the sulfate adsorption kinetic on EWFs [29,32]. Besides, at the equilibrium, a good correlation is found between the calculated adsorbed amount, Q_e , and the experimental one.

3.5. Thermodynamic study of EWFs

To assess the energetic aspects of the adsorptive process, the thermodynamic parameters including the adsorption change in Gibbs free energy ΔG° (kJ mol^{-1}) Eq. (15), the enthalpy ΔH° (J mol^{-1}) and the entropy ΔS° ($\text{J mol}^{-1} \text{ K}^{-1}$) Eq. (16), of the

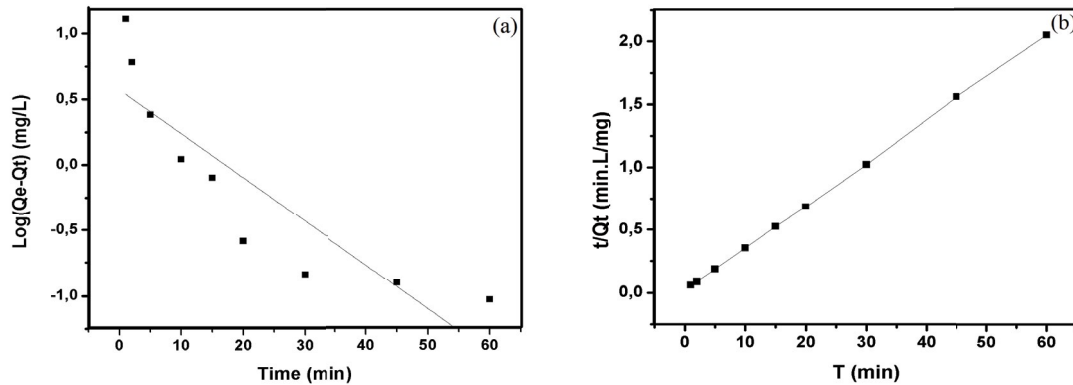


Fig. 12. (a) Pseudo-first-order kinetic and (b) pseudo-Second-order kinetic for SO_4^{2-} removal.

Table 4
Kinetic parameters

Adsorption kinetic modeling					
Pseudo-first-order			Pseudo-second-order		
k_1 (min^{-1})	Q_e (mg g^{-1})	R^2	k_2 ($\text{g mg}^{-1} \text{min}^{-1}$)	Q_e (mg g^{-1})	R^2
0.13	6.71	0.93	0.05	53.92	0.99

adsorption were determined using, respectively, the slope and the intercept of the Van't Hoff linear equation [12,34]:

$$\Delta G^\circ = -RT \ln K_C \quad (15)$$

$$\ln K_C = -\frac{\Delta H^\circ}{RT} + \frac{\Delta S^\circ}{R} \quad (16)$$

where $K_C = Q_e/C_e$. K_C (L mg^{-1}) is the Langmuir isotherm constant, R ($8.314 \text{ J mol}^{-1}\text{K}^{-1}$) is the universal gas constant; T (K) is the absolute solution temperature. Note that the temperature in the adsorption experiment varied from 4°C (277.15 K) to 40°C (313.15 K). Also, taken into account the fact that the unit of ΔG° is J mol^{-1} and the unit for the term RT is in J mol^{-1} , therefore, the equilibrium constant K_C in Eq. (15) must be dimensionless. Furthermore, according to the literature, the adsorption free energy change is generally obtained, in straight way by using Eq. (15) and by expressing K_C in various units (L mol^{-1} , L g^{-1} , mL mg^{-1} , etc.). As results, the calculated values for enthalpy ΔH° and entropy ΔS° are not correct. Therefore, a rigorous ΔG° calculation should use dimensionless K_C values in Eq. (17). Thus, if the K_C value is expressed in L mol^{-1} , it should be multiplied by 55.5 (number of water moles per liter of solution) to make it a dimensionless constant. Thus, the correct ΔG° value can be obtained from Eq. (17):

$$\Delta G^\circ = -RT \ln (55.5 K) \quad (17)$$

If the K_C value is given in L g^{-1} , and taking into account the fact that the density of the solution is $\approx 1 \text{ g mL}^{-1}$, K_C should be multiplied by 1,000 ($1 \text{ L} = 1,000 \text{ mL}$), to make it a dimensionless constant [36].

Table 5
Thermodynamic parameters

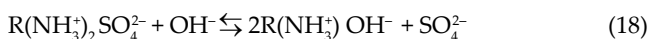
T (K)	ΔG° (kJ mol^{-1})	ΔS° ($\text{J mol}^{-1} \text{K}^{-1}$)	ΔH° (kJ mol^{-1})
277.15	-6.19		
283.15	-6.88	39.34	4.35
293.15	-8.15		
313.15	-7.44		

In the present work, the calculated thermodynamic parameters for the sulfate adsorption are reported on Table 5. As can be seen on this table, the enthalpy ΔH° is positive, suggesting that the adsorption process is endothermic. The low value of this heat measurement ($<40 \text{ kJ mol}^{-1}$) shows that the adsorption is physical in nature. Further, the positive ΔS° values show that the sulfates removal is accompanied by a disorder increase on the fiber surface. These results indicate that the sulfate molecules adsorbed on the EWFs surface, are more randomly distributed on the solid surface, as compared to their presence in the bulk aqueous phase. Finally, the negative value of ΔG° indicates that the adsorption of SO_4^{2-} from water onto EWFs is spontaneous [34].

3.6. Regeneration of EWFs

The earlier detailed adsorption–desorption experiments were conducted to evaluate both the adsorption reversibility and the adsorbent regeneration feasibility. The results indicate that up to 66%, 50% and 45% for SO_4^{2-} can be recovered, respectively, at $\text{pH} = 9$, $\text{pH} = 7$ and $\text{pH} = 4$ (Fig. 13). It is obvious that the sulfate recovery increase results from the aqueous phase pH increase. Thus, as the pH increases, the generated OH^- ions preferentially interact with the protonated

amino groups, exchanging hence with the adsorbed SO_4^{2-} ions present on the fiber surface Eq. (18). Subsequently, the amino groups are deprotonated according to Eq. (19), and the fiber surface loses its positive sites leading to the release of sulfate ions to the aqueous phase [28]. It should be noted that in the present work, the regeneration cycles were examined for the recovery at optimal value of $\text{pH} = 9$. As can be seen in Fig. 14, the elimination percentage has decreased with subsequent adsorption-desorption cycles (27.07% to 8.35% and 66.28% to 3% for adsorption and desorption respectively), this may be due to accumulation of incomplete desorption of sulfate ions from the surface of EWFs.



3.7. Comparison study

Several works reported in the literature have used different adsorbents, such as polypyrrole modified activated carbons, poly(m-phenylenediamine), protonated grafted-chitosan and chitin-based shrimp shells to remove SO_4^{2-} ions from aqueous solutions. In Table 6 are gathered the values of the maximum adsorption capacities of sulfate ions obtained by using various adsorbents. The best result are obtained by using chitin-based shrimp shells, as adsorbent, which leads to a maximum adsorption capacity of 156 mg g^{-1} [28], followed by 108.5 mg g^{-1} for poly(m-phenylenediamine) [35] and 107.53 mg g^{-1} for protonated grafted-chitosan [37]. However, the lowest adsorbed sulfate amount, 44.7 mg g^{-1} is obtained by using polypyrrole modified activated carbon as adsorbent [34]. Despite these findings, and taking into account the significant costs and the difficulties to use these various adsorbents, the use of natural and low cost adsorbent such as the wool fibers seems to be an appropriate alternative for sulfate removal from water.

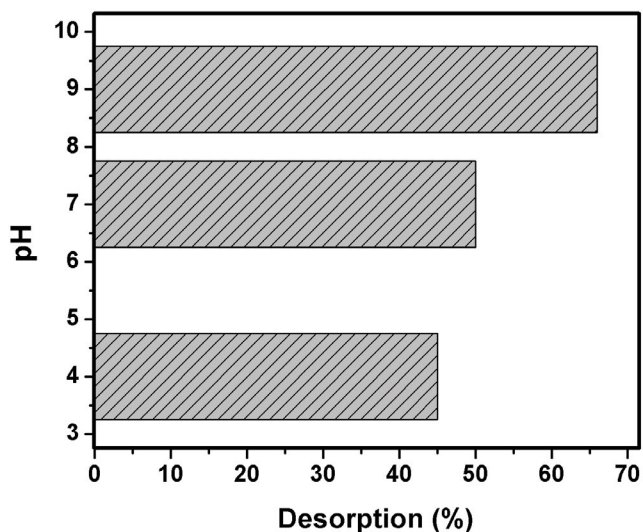


Fig. 13. SO_4^{2-} desorption efficiency from EWFs ($T = 25^\circ\text{C}$, 10 g L^{-1} , $t = 60 \text{ min}$).

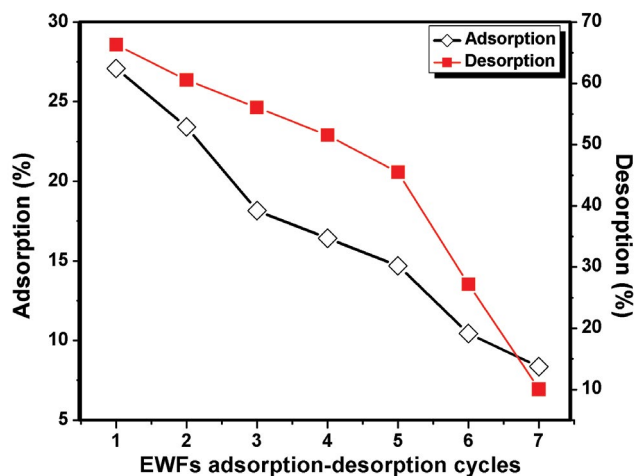


Fig. 14. Adsorption-desorption cycles (Optimum conditions for: adsorption ($[\text{SO}_4^{2-}] = 1,000 \text{ mg L}^{-1}$; $T = 25^\circ\text{C}$; $\text{pH} = 2$; $t = 20 \text{ min}$, 5 g L^{-1}), desorption ($\text{pH} = 9$; $T = 25^\circ\text{C}$, 10 g L^{-1} ; $t = 60 \text{ min}$).

Table 6

Comparison of the sulfate adsorption capacities using different adsorbents

Type of adsorbent	Q_m (mg g^{-1})	Reference
Polypyrrole modified activated carbons	44.7	[34]
Poly(m-phenylenediamine)	108.5	[35]
Protonated grafted-chitosan	107.53	[37]
Chitin-based shrimp shells	156	[28]
Esterified wool fibers (EWFs)	123.08	In this study

4. Conclusion

In the present work, it was shown that both RWFs and EWFs with methanol by using HCl, as a catalyst, are efficient in removing sulfate ions from aqueous solutions. However, the EWFs adsorbent was found to have a better adsorption capacity as compared to RWFs. The parameters affecting the sulfate removal such as the initial pH, initial adsorbate concentration, the adsorbent amount, and the temperature were investigated. The data indicate that $\text{pH} = 2$ was the optimal pH value for sulfate removal on both RWFs and EWFs. Further, at optimal adsorbate concentration ($1,000 \text{ mg L}^{-1}$) it was found that the appropriate times needed for sulfate removal from water onto EWFs and RWFs, were, respectively, 20 and 30 min. For the complete sulfate removal from water onto EWFs and RWFs, respectively, 6 and 11 g of the adsorbent were needed.

Regarding the theoretical trends of the sulfate removal from water onto the EWFs adsorbent, a good correlation was found between the experimental data and the Langmuir model predicting a maximum adsorption capacity of 123.08 mg g^{-1} . Further, the kinetic sulfate adsorption was well described the pseudo-second-order model. Finally, the assessment of the thermodynamic parameters

revealed that the sulfate adsorption from water onto EWFs was a spontaneous and an endothermic process. The overall data show that the wool fibers are good natural alternative for high removal capacity of sulfate from water. However, the highest removed sulfate amount was obtained by using the modified wool fibers. Finally, both experimental and theoretical adsorption data have confirmed that the ion exchange fibers, used in the present work, are appropriate adsorbent for sulfate removal from water, and can be regenerated.

Acknowledgments

The authors gratefully acknowledge Said GMOUH, Professor at Faculty of Sciences Ben M'Sik at Hassan II University, for his scientific and technical contribution. In addition, the textile research laboratory direction (REMTEX) from the Higher School of Textile and Clothing Industries (ESITH) for its financial support and technical assistance, as well as the Ain Chock Faculty of Sciences.

Symbols

C_b	—	Initial concentration of the base, NaOH
C_a	—	Concentration of the acid solution, HCl used in the titration experiments
V_b	—	Initial volume of the base, NaOH
V_a	—	Volume of the acid solution, used in the titration experiments
C_0	—	Initial concentration
C_e	—	Equilibrium concentration
Q_e	—	Equilibrium adsorbed amount
Q_{max}	—	Maximum adsorbed amount
K_L	—	Equilibrium constant relative to the Langmuir model
K_F	—	Equilibrium constant relative to the Freundlich model
R_L	—	Separation factor
β	—	Constant related to the mean free sorption energy
E, ε	—	Polanyi potential
R	—	Gas constant
T	—	Absolute solution temperature
Q_t	—	Amount adsorbed at time t
k_1	—	Rate constant of first-order adsorption reaction
k_2	—	Rate constant of second-order adsorption reaction
ΔG°	—	Gibbs free energy
ΔH°	—	Enthalpy
ΔS°	—	Entropy
K_C	—	Langmuir model constant

References

- [1] W. Tang, D. He, C. Zhang, T.D. Waite, Optimization of sulfate removal from brackish water by membrane capacitive deionization (MCDI), *Water Res.*, 121 (2017) 302–310.
- [2] E. Pons-Branchu, M. Roy-Barman, L. Jean-Soro, A. Guillerme, P. Branchu, M. Fernandez, E. Dumont, E. Douville, J.-L. Michelot, A.M. Phillips, Urbanization impact on sulfur content of groundwater revealed by the study of urban speleothem-like deposits: case study in Paris, France, *Sci. Total Environ.*, 579 (2017) 124–132.
- [3] D.R. Mulinari, M.L.C.P. da Silva, Adsorption of sulphate ions by modification of sugarcane bagasse cellulose, *Carbohydr. Polym.*, 74 (2008) 617–620.
- [4] F. Liang, Y. Xiao, F. Zhao, Effect of pH on sulfate removal from wastewater using a bioelectrochemical system, *Chem. Eng. J.*, 218 (2013) 147–153.
- [5] S. Tait, W.P. Clarke, J. Keller, D.J.J.W.R. Batstone, Removal of sulfate from high-strength wastewater by crystallisation, *Water Res.*, 43 (2009) 762–772.
- [6] B. Sadeghalvad, A. Azadmehr, A. Hezarkhani, Sulfate decontamination from groundwater by metal layered double hydroxides functionalized high phosphorus iron ore waste as a new green adsorbent: experimental and modeling, *Ecol. Eng.*, 106 (2017) 219–230.
- [7] N. Arahman, S. Mulyati, M.R. Lubis, R. Takagi, H. Matsuyama, Removal profile of sulfate ion from mix ion solution with different type and configuration of anion exchange membrane in electro dialysis, *J. Water Process. Eng.*, 20 (2017) 173–179.
- [8] W. Dou, Z. Zhou, L.-M. Jiang, A. Jiang, R. Huang, X. Tian, W. Zhang, D. Chen, Sulfate removal from wastewater using ettringite precipitation: magnesium ion inhibition and process optimization, *J. Environ. Manage.*, 196 (2017) 518–526.
- [9] F. Amaral, M. Kato, L. Florêncio, S.J.B.t. Gavazza, Color, organic matter and sulfate removal from textile effluents by anaerobic and aerobic processes, *Bioresour. Technol.*, 163 (2014) 364–369.
- [10] J. Lopez, M. Reig, O. Gibert, C. Valderrama, J.J.D. Cortina, Evaluation of NF membranes as treatment technology of acid mine drainage: metals and sulfate removal, *Desalination*, 440 (2018) 122–134.
- [11] L. Pino, C. Vargas, A. Schwarz, R.J.C.E.J. Borquez, Influence of operating conditions on the removal of metals and sulfate from copper acid mine drainage by nanofiltration, *Chem. Eng.*, 345 (2018) 114–125.
- [12] A. Saber, M. Tafazzoli, S. Mortazavian, D.E. James, Investigation of kinetics and absorption isotherm models for hydroponic phytoremediation of waters contaminated with sulfate, *J. Environ. Manage.*, 207 (2018) 276–291.
- [13] Z. Hanzlikova, J. Braniša, K. Jomová, M. Fueleop, P. Hybler, M.J.S. Porubská, P. Technology, Electron beam irradiated sheep wool—prospective sorbent for heavy metals in wastewater, *Sep. Purif. Technol.*, 193 (2018) 345–350.
- [14] L. Zhang, Q. Zhai, X. Zhao, X. Min, Q. Zhu, J. Li, Modified wool-iron biopolymer-based complex as an active heterogeneous decontamination photocatalyst, *J. Energy Chem.*, 25 (2016) 1064–1069.
- [15] G. Giri, P.K. Sahoo, R.K. Samal, Graft copolymerization onto wool fibers: grafting of acrylamide onto wool fibers initiated by potassium monopersulphate/Fe (II) redox system, *J. Appl. Polym.*, 40 (1990) 471–483.
- [16] H.H. Ghafar, T. Salem, E.K. Radwan, A.A. El-Sayed, M.A. Embaby, M.J. Salama, Modification of waste wool fiber as low cost adsorbent for the removal of methylene blue from aqueous solution, *Egypt J. Chem.*, 60 (2017) 395–406.
- [17] H. Zhang, Z. Yang, X. Zhang, N. Mao, Photocatalytic effects of wool fibers modified with solely TiO₂ nanoparticles and N-doped TiO₂ nanoparticles by using hydrothermal method, *Chem. Eng.*, 254 (2014) 106–114.
- [18] D.J. Kilpatrick, J.A. Maclaren, The dyeing properties of esterified wools, *Text. Res. J.*, 39 (1969) 279–283.
- [19] E. Moaseri, M. Baniadam, M. Maghrebi, M. Karimi, A simple recoverable titration method for quantitative characterization of amine-functionalized carbon nanotubes, *Chem. Phys. Lett.*, 555 (2013) 164–167.
- [20] J. Rodier, *L'analyse de l'eau*, Duno, 2009, pp. 363–364.
- [21] V.K. Gupta, A. Rastogi, A. Nayak, Adsorption studies on the removal of hexavalent chromium from aqueous solution using a low cost fertilizer industry waste material, *J. Colloid Interface Sci.*, 342 (2010) 135–141.
- [22] D. Pasquini, M.N. Belgacem, A. Gandini, A.A. Curvelo, Surface esterification of cellulose fibers: characterization by DRIFT and contact angle measurements, *J. Colloid Interface Sci.*, 295 (2006) 79–83.

- [23] M.M. Hassan, L. Schiermeister, M.P. Staiger, Thermal, chemical and morphological properties of carbon fibres derived from chemically pre-treated wool fibres, *RSC Adv.*, 5 (2015) 55353–55362.
- [24] M.E.A. Manaf, M. Tsuji, S. Nobukawa, M. Yamaguchi, Effect of moisture on the orientation birefringence of cellulose esters, *Polymer*, 3 (2011) 955–966.
- [25] D.R. Rao, V.B. Gupta, Thermal characteristics of wool fibers, *J. Macromol. Sci.*, 31 (1992) 149–162.
- [26] E. Protopopoff, P. Marcus, Potential–pH diagram for sulfur and hydroxyl adsorbed on silver in water containing sulfides, *Electrochim. Acta*, 63 (2012) 22–27.
- [27] H. Bouchoum, D. Benmoussa, A. Jada, M. Tahiri, O. Cherkaoui, Synthesis of amidoximated polyacrylonitrile fibers and its use as adsorbent for Cr(VI) ions removal from aqueous solutions, *Environ. Prog. Sustainable Energy*, 31 (2019), <https://doi.org/10.1002/ep.13196>.
- [28] A. Moret, J. Rubio, Sulphate and molybdate ions uptake by chitin-based shrimp shells, *Miner. Eng.*, 16 (2003) 715–722.
- [29] B. Cojocariu, A.M. Mocanu, G. Nacu, L. Bulgariu, Possible utilization of PET waste as adsorbent for Orange G dye removal from aqueous media, *Desal. Water Treat.*, 104 (2018) 338–345.
- [30] G. Mahmoud, M. Abdel Khalek, E. Shoukry, M. Amin, A. Abdulghany, Removal of phosphate ions from wastewater by treated hydrogel based on chitosan, *Egypt. J. Chem.*, 62 (2019) 1537–1549.
- [31] H.H. Abdel Ghafar, M.A. Embaby, E.K. Radwan, A.M. Abdel-Aty, Biosorptive removal of basic dye methylene blue using raw and CaCl₂ treated biomass of green microalga *Scenedesmus obliquus*, *Desal. Water Treat.*, 81 (2017) 274–281.
- [32] S.T. El-Wakeel, E.K. Radwan, H.H.A. Ghafar, A.S. Moursy, Humic acid-carbon hybrid material as lead(II) ions adsorbent, *Desal. Water Treat.*, 74 (2017) 216–223.
- [33] M.A. Embaby, H.H.A. Ghafar, M.M.E. Shakhdofo, N.M. Khalil, E.K. Radwan, Removal of iron and manganese from aqueous solution using some clay minerals collected from Saudi Arabia, *Desal. Water Treat.*, 65 (2017) 259–266.
- [34] S. Hong, F.S. Cannon, P. Hou, T. Byrne, C. Nieto-Delgado, Adsorptive removal of sulfate from acid mine drainage by polypyrrole modified activated carbons: effects of polypyrrole deposition protocols and activated carbon source, *Chemosphere*, 184 (2017) 429–437.
- [35] P.-I. Sang, Y.-y. Wang, L.-y. Zhang, L.-y. Chai, H.-y. Wang, Effective adsorption of sulfate ions with poly(*m*-phenylenediamine) in aqueous solution and its adsorption mechanism, *Trans. Nonferrous Met. Soc. China*, 23 (2013) 243–252.
- [36] S.K. Milonjić, A consideration of the correct calculation of thermodynamic parameters of adsorption, *J. Serb. Chem. Soc.*, 72 (2007) 1363–1367.
- [37] G. Yingjuan, X. Juanqin, B. Qiang, D. Yewei, Z. Meina, Adsorption of sulfate onto protonated grafted-chitosan from aqueous solution, *Chin. J. Environ. Eng.*, 10 (2013) 6.